World Conference on
Timber Engineering
Oslo 2023

GLUED-LAMINATED TIMBER BEAMS WITH LARGE ROUND HOLES: AN EXPERIMENTAL AND NUMERICAL INVESTIGATION

Francesco Mirko Massaro[1], Kjell Arne Malo[2]

ABSTRACT: Timber beams are oftentimes used as joists in timber floors. Especially for small timber buildings like two-story housing for single or few families, it may be necessary to let service pipes pass through the joists to avoid a reduction of the story height. Therefore, there is a need to have large holes in the timber joists, which under the current local guidelines and the future European regulations, leads to the use of timber beams of significant height. In this study, the capacity of glued-laminated timber beams with large round holes is evaluated. The paper presents results from novel experiments performed on beams with round holes positioned in two different configurations. The holes are considered as large, i.e. the diameter of the holes is 50% of the timber beam height or larger. The objectives are, in addition to the experimental investigations, to establish a numerical simulation approach of these experiments which can be used to future studies of possible solutions to the challenge of large holes in timber joists. For comparison, an analytical evaluation of the beams capacity in accordance with the future European regulations is added.

KEYWORDS: timber beams, large holes, glulam, numerical modelling, cohesive zone

1 INTRODUCTION

Timber is one of the most used structural materials because of its excellent mechanical properties. Moreover, due to its advantage of being environmental friendly, there has been a renewed interest in its usage. In the recent years, examples of buildings such as Treet and Mjøstårnet, both in Norway, have shown that timber can be a good material choice also for high-rise structures [1, 2]. However, for the Nordic timber industry the use of timber in houses for single and few families is still more important. The flooring in these smaller building consists usually of traditional joisted floors with simple solutions for ceiling and decking of the floors, as acoustic properties are of little relevance within single apartments. In these buildings, it is preferable to let pipes, used by e.g. water, heating, or ventilation systems, pass through beams in the floors to reduce the height of the building. The design criteria for these types of floors are usually deformations and vibrations, and one or two large holes in the beams, larger than half of the height, do not increase the deformation significantly, as the portion of the beams having reduced bending stiffness will be very small. Nevertheless, it is a very cheap improvement to reduce the spacing of the beams, in areas where the beams have large holes, to compensate for the reduction in stiffness and strength. Therefore, the presence of large holes for pipes in timber beams is very beneficial and leads to effective building systems without unnecessary use of material and space. The presence of holes generates concentrations of shear and tensile stresses orthogonal to grain in proximity of the hole. The exact location of the stress concentrations depends on the acting forces on the member, i.e. on the ratio between the bending moment M and the shear force V in the hole section (see Figure 1).

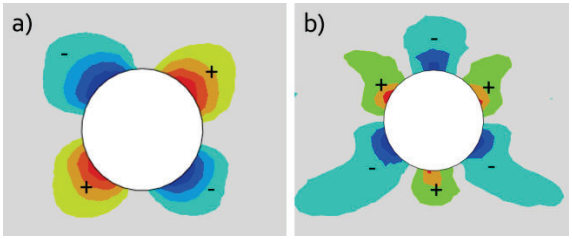

Figure 1: *Stress concentration around circular holes: a) dominant shear (M/V=1h where h is the beam height), b) pure bending (M/V=∞). The symbols + and – indicate tension and compression, respectively.*

Aicher and Höfflin [3] have studied the location of the stress concentrations around a circular hole in a beam subjected to various loading modes, concluding that at approximately 45° from the center of the hole, stress concentrations occur at the edge of the hole.
The strength of timber in tension perpendicular to grain is relatively small and therefore the stress concentrations lead to a reduction of the capacity of the timber element. Consequently, the design of timber members with holes is challenging. Indeed, Eurocode 5 [4] still does not include any normative rule about the presence of holes in timber beams. Nonetheless, there exist national regulations, such as the German National Annex to Eurocode 5 [5], or local guidelines [6] that provide an indication on the maximum hole size. An overview on recent developments on design guidelines can be found in Tapia and Aicher [7].

[1] Francesco Mirko Massaro, NTNU Norwegian University of Science and Technology, Norway, francemm@ntnu.no
[2] Kjell Arne Malo, NTNU Norwegian University of Science and Technology, Norway

https://doi.org/10.52202/069179-0307

Moreover, the future generation of Eurocode 5 will include normative rules, based on Danzer et al. [8], about the design of timber members with holes, although the diameter of the hole, *d*, will be limited to 30% of the timber beam height, *h*, if unreinforced [9]. For joisted floors in small wooden houses, the height of the joists is in the range of 220 mm to 300 mm. Typical water pipes in buildings can have diameter of about 160 mm and thus the limitation on the ratio *d*/*h* increases the necessary beam height significantly with the presence of a hole.

Numerous experiments have been performed on glued-laminated timber beams with round holes over the time, i.a. Johannesson [10], Höfflin [11], Aicher and Höfflin [12], Danzer et al. [13]. However, in these studies the diameter of the holes was always smaller than 50% of the beam height.

Several methods were proposed to analyze the failure load of timber beams with holes, such as i.a. models based on linear elastic fracture mechanics (LEFM) [14], Weibull based models [15, 16], cohesive zone models (CZM) [17]. The use of numerical models with cohesive elements has provided good accuracy in the evaluation of the failure load of timber structural elements, such as for laminate veneer lumber (LVL) beams with round holes [18] and glulam beams with rectangular holes [19].

The main objectives of the present study are to evaluate the experimental capacity and a numerical model of glued-laminated timber beams with large round holes. In this study, a hole is defined as large by having a diameter larger than 50% of the beam height. Thus, novel experiments on timber beams with large round holes were performed. The experimental results were then used to validate the numerical model using cohesive elements with definition of a traction-separation law. Finally, an analytical evaluation of the failure load of timber beams with large round holes, based on the latest draft of the new generation of Eurocode 5, is provided.

2 MATERIAL AND METHODS

2.1 EXPERIMENTS

The experimental investigation was carried out on glued-laminated beams with large holes at the Norwegian University of Science and Technology, Trondheim. The experiments were conducted on K-beams made of Norway Spruce (Picea abies). The K-beams, manufactured by Inntre Kjeldstad AS, are not covered by the EN 14080:2013 standard [20], and therefore they have their own technical approval [21]. Their inner lamellae, classified as LT20 according to the INSTA 142:2009 standard [22], are 17 or 19 mm thick, while the two outermost lamellae are 47 mm thick and are classified as C24 according to the EN 338:2016 standard [23].

Sixty-nine tests were conducted on beams with dimension 36×300×4200 mm^3. Sixty of the tested beams have a hole of 150 to 170 mm diameter, which corresponds to 50 to 56.7% of the beam height. The series name reflects the position and the diameter of the hole: M indicates that the hole is located in a moment-dominated zone, while V indicates that the hole is located in a shear-dominated zone. Moreover, an additional series of nine experiments on K-beams without holes was performed and it is denominated with the letter K. An overview of the performed experiments is given in Table 1 and the geometrical properties are explained in Figure 2.

***Table 1**: Summary of the performed experiments*

Series name	n. of tests	*d* [mm]	l_V [mm]	l_A [mm]	l_L [mm]
M170	9	170	1630	1530	300
V170	10	170	700	600	1230
M160	11	160	1640	1540	300
V160	10	160	700	600	1240
M150	10	150	1650	1550	300
V150	10	150	700	600	1250
K	9	-	-	-	-

The beams were tested with a 3-point bending configuration (see Figure 2), with the supports centered at 100 mm from the beam ends. Prior to testing, the glulam beams were located in a room with the constant climate of 20 °C of temperature and 65% relative humidity (RH) of the air for the time necessary to reach a moisture content (MC) of approximately 12% in the beams.

The load was applied by means of a hydraulic actuator and it was distributed over an aluminum U-profile 140 mm long and 4 mm thick, to avoid local compression deformation (see Figure 2). Moreover, the load was continuously recorded by the test machine together with the displacement of the actuator.

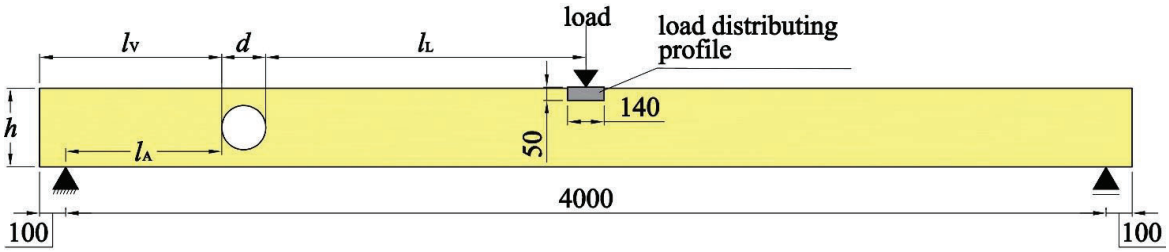

***Figure 2:** Test setup with location of the hole and the load.*

https://doi.org/10.52202/069179-0307

The tests were conducted in displacement control and performed in agreement with the standard EN 380:1993 [24] for the determination of the load at failure. After an initial loading/unloading cycle with the force cycling between ca. 1 and 2 kN, the displacement is increased and then kept constant in order to reach and maintain a loading force of ca. 3 kN. Finally, the displacement is further increased until the failure of the beam is obtained.

2.2 NUMERICAL SIMULATIONS

A numerical model to simulate the behavior of the glulam beams was developed in the FEM software program Abaqus [25].

Timber can be considered as an orthotropic material. However, in the two transversal directions the same material properties were used. Nevertheless, it should be noted that the shear moduli are independent from the normal moduli and thus the material was modeled differently from transversally isotropic. The normal moduli E_x, E_y, E_z and the shear moduli G_{xy}, G_{xz} are chosen according to the K-beams technical approval [21], while G_{yz} as 1/10 of the other shear moduli, and the Poisson's ratios are selected based on Dahl [26] and Massaro et al. [27]. The elastic material properties used in the numerical model are given in Table 2, where the subscript "x" indicates the grain direction. The coordinate system is depicted in Figure 3.

The geometry of the model resembles the geometry of the tested beams, i.e. the model consists of a beam, 4200 mm long and cross-section of 36×300 mm^2. The beam has a hole located according to the geometry given in Table 1 and illustrated in Figure 2.

The beam movements in the y-direction are on the supports on the bottom beam surface, centered at 100 mm from the ends of the beam as displayed in Figure 3b, resembling the experimental supports. The beam is loaded by applying a displacement on a 36×140 mm^2 surface on the middle of the beam top surface, i.e. in the xz-plane (Figure 3a). The loading surface resembles the load distributing area of the experimental configurations.

The behavior in compression parallel to grain is considered to be elastic-perfectly plastic, with elastic limit $f_{c,0}$ (see Table 2). Moreover, the location of the highest transversal tensile stresses around the hole, as determined with an elastic analysis for each configuration, is at the hole edge in a plane at approximatively 40° - 60° from the center of the hole. In correspondence of the highest transversal stress, cohesive layers (layers A and B in Figure 3a), crossing the entire length of the beam, were then introduced in the model. An additional cohesive layer (layer C) is located vertically under the hole, as this area may be subjected to high tensile stress parallel to grain due to bending (see Figure 3a).

A cohesive layer requires the definition of a traction-separation law, i.e. stiffness properties, a damage initiation criterion and a damage evolution phase. The traction-separation law used in this model is a bilinear law, with an initial elastic phase succeeded by a linear softening which starts when the chosen damage initiation criterion is fulfilled (see Figure 4).

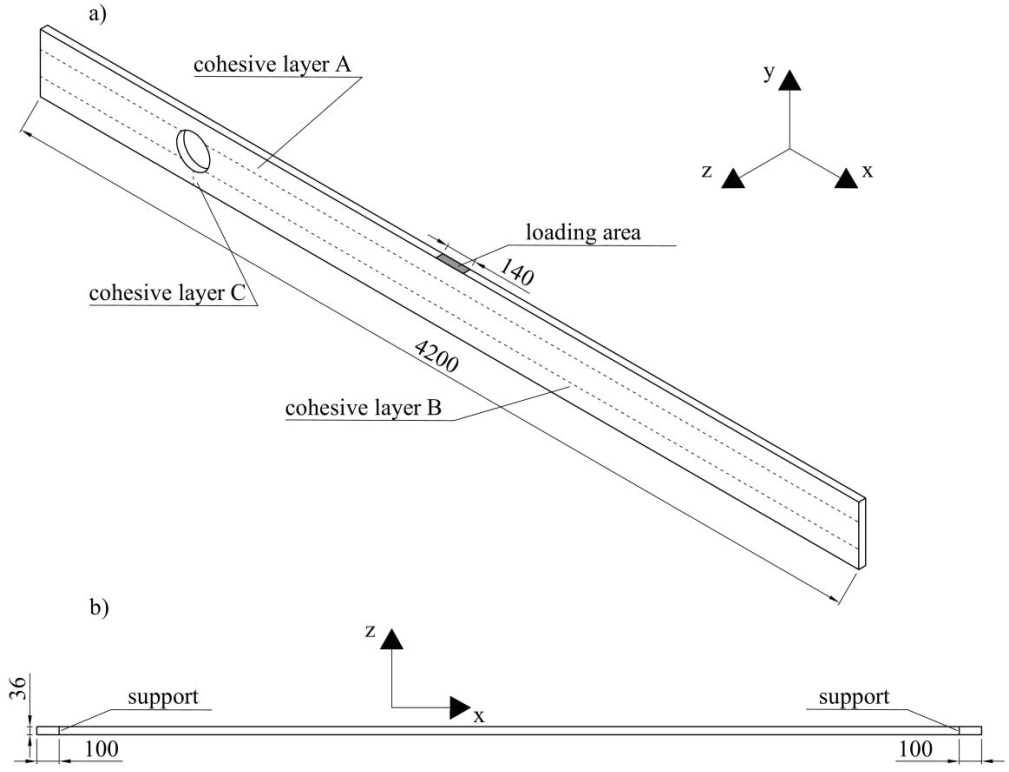

Figure 3: *Geometry of numerical model: a) isometric view and location of the cohesive layers, b) bottom plan view*

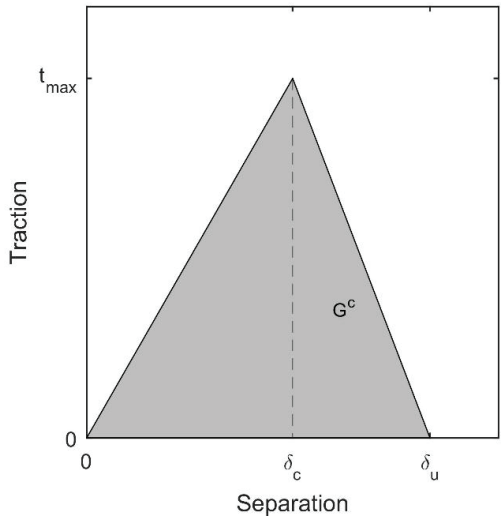

Figure 4: *Traction-separation law*

The elastic stiffness values of the cohesive layers are equal to the stiffness values used for the timber parts. As damage initiation criterion, the maximum stress criterion has been used, i.e. the damage starts when either the tensile stress orthogonal to the cohesive layer or the shear stress in the layer reaches the maximum allowed value. The criterion is expressed as in Equation (1), where t_n, t_s, t_t represent the normal and the two shear tractions, respectively. Note that the angular brackets specify that t_n is a tension stress and can thus only be positive. The subscript max indicates the elastic limit stress in the specific direction. These limit values are chosen as the mean values of the respective strengths.

$$\max\left\{\frac{\langle t_n\rangle}{t_{n\max}};\frac{t_s}{t_{s\max}};\frac{t_t}{t_{t\max}}\right\}=1 \qquad (1)$$

The mean values for shear and tension parallel to grain strength have been obtained from the results of the experiments performed by Treteknisk [28-30] on the K-beams. On the other hand, the tension orthogonal to grain mean strength has been assumed based on Dahl [26] and Massaro et al. [27], while the compression parallel to grain mean strength was based on the K-beams Technical Approval [21, 31].

The damage evolution phase in the layers A and B is controlled by the energy method with linear softening [18, 32]. The critical values of the fracture energy for the opening mode (mode I) and shearing mode (mode II) are chosen as the average of the values reported by Ostapska [33] and Ostapska and Malo [34]. Furthermore, the mixed mode, usually relevant in beams with holes, is here described by Wu's criterion [35, 36] presented in Equation (2).

$$\left(\frac{G_I}{G_{Ic}}\right)^{0.5}+\frac{G_{II}}{G_{IIc}}=1 \qquad (2)$$

In Equation (2), G_I and G_{II} represent the fracture energies for mode I and mode II, respectively, while G_{Ic} and G_{IIc} denote the respective critical values.

The material properties of wood and of the cohesive layers are summarized and given in Table 2.

Table 2: *Material properties of wood and of the cohesive layers used in numerical simulations*

Elastic properties of wood	Normal moduli	E_x	11000 MPa	[21]
		$E_y \equiv E_z$	370 MPa	
	Shear moduli	$G_{xy} \equiv G_{xz}$	690 MPa	
		G_{yz}	69 MPa	[20]
	Poisson's ratios	ν_{xy}	0.5	[26, 27]
		ν_{xz}	0.6	
		ν_{yz}	0.6	
Mean strengths	Tension orthogonal to grain	$f_{t,90}$	2 MPa	[26, 27]
	Tension parallel to grain	$f_{t,0}$	40 MPa	[29, 30]
	Shear	f_v	4 MPa	[28]
	Compression parallel to grain	$f_{c,0}$	26 MPa	[21, 31]
Fracture energies (layers A and B)	Mode I	G_{Ic}	0.24 N/mm	[33, 34]
	Mode II	G_{IIc}	0.79 N/mm	[33]

The elements in the cohesive layer C followed a different damage evolution since they have to represent tensile failure parallel to grain. These elements, if the damage initiation criterion is satisfied, immediately lose their stiffness. This is obtained by imposing $\delta_u \cong \delta_c$ as their damage evolution law (see Figure 4).

Eight-node three-dimensional elements were used in the model: C3D8 (i.e. full integration) for the wooden material and COH3D8 for the cohesive layers with viscous parameter chosen equal to 10^{-3} [18]. Note that the viscous parameter is only necessary to ensure convergence of the analysis and does not have physical meaning. After a sensitivity mesh study, the mesh size has been chosen equal to 20 mm for the timber parts, and equal to 5 mm for the cohesive layers, thus in agreement with Abaqus guidelines [25].

https://doi.org/10.52202/069179-0307

3 RESULTS AND DISCUSSION

3.1 EXPERIMENTAL RESULTS

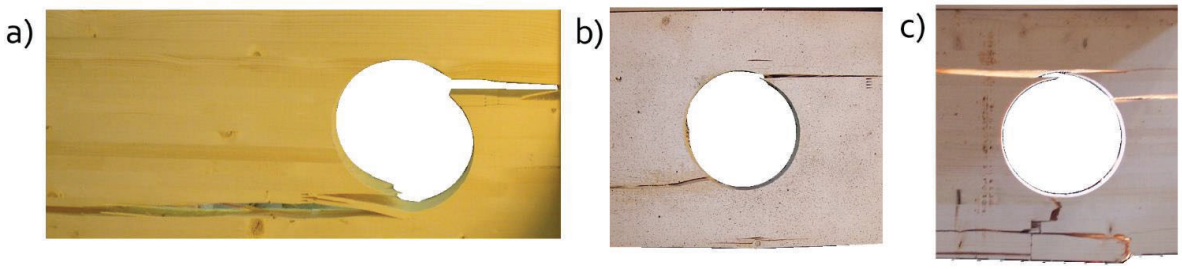

***Figure 5**: Examples of beams at failure: a) Test V170-5; b) Test M150-1; c) Test M150-4*

Figure 5 shows typical examples of beam failure. The cracks were usually initiating either at the top right or at the bottom left of the hole circumference, and then they propagated from there, usually until the beam ends. It should be noted that some beams of the M-series presented additional cracks on the bottom chord of the beam (see e.g. Figure 5c), likely due to bending stresses and thus tension parallel to grain. The failure load F_f, i.e. the maximum load reached in an experimental test, for each tested beam is given in Figure 6, together with the mean value of the series.

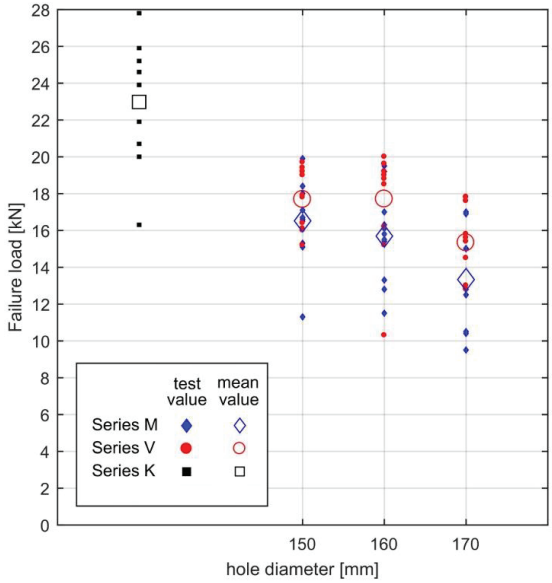

***Figure 6:** Experimental failure loads.*

In Figures 7 and 8, the red dashed lines depict a typical representative outcome of the results of the conducted investigation, described in Chapter 2.1, for the series with the largest holes, i.e. M170 and V170, respectively. The response is given by loading force vs. displacement.
The results show, after the initial loading/unloading phase, a linear increase of the loading force with respect to the deformation applied in agreement with loading procedure described in Chapter 2.1. By increasing the load, the first crack appeared and it gradually spread over the whole beam thickness. Thus, the corresponding load is defined as cracking load (F_{cr}). Afterwards, the crack propagated and new cracks were formed, until a sudden drop in the force occurs corresponding to failure. In some cases, especially in the M-series, the loading force increased again after the first drop, probably because of the presence of knots and finger joints or fiber bridging, but it was followed again by further sudden drops in the force, thus reaching failure.
The distribution of the failure load may be considered lognormal [37]. Thus, the mean and characteristic values of the measured cracking loads, $F_{cr,mean}$ and $F_{cr,k}$ respectively, and failure loads, $F_{f,mean}$ and $F_{f,k}$ respectively, were then determined according to EN14358. The values are reported in Table 3.

***Table 3:** Experimental results: mean and characteristic values. (Values in kN. Coefficient of variation in parentheses.)*

Series	$F_{cr,mean}$	$F_{cr,k}$	$F_{f,mean}$	$F_{f,k}$
M170	11.03 (0.323)	5.37	13.33 (0.220)	8.20
V170	12.70 (0.094)	10.41	15.33 (0.134)	11.50
M160	13.02 (0.169)	9.05	15.69 (0.162)	11.12
V160	15.56 (0.559)	4.35	17.70 (0.206)	11.34
M150	12.70 (0.286)	6.62	16.52 (0.154)	11.85
V150	13.44 (0.221)	8.14	17.68 (0.094)	14.46
K	-	-	22.97 (0.165)	16.00

The results in Table 3 and Figure 6 show that the failure load of the M-series is lower than in the V-series, arguably due to high tensile stress parallel to grain under the hole, in addition to the stress concentrations around the hole. Indeed, the reduction of the mean failure load, from the

reference value for beams without holes (i.e. K-series), ranges between 23% and 33% for the V-series, while for the M-series it ranges between 28% and 42%. The difference between the failure load of the M-series and the V-series is in the order of 2 kN. Moreover, the V-series seems to be less affected than the M-series by the presence of larger holes. Indeed, increasing the diameter of the hole from 150 mm to 170 mm, i.e. from $d/h = 0.5$ to $d/h = 0.57$, the beams of the M-series observe a reduction of the failure load of about 19%, while the reduction is lower for the V-series beams, i.e. approximately 13%.

3.2 NUMERICAL RESULTS

The numerical simulations of the timber beams were performed with the parameters given in Chapter 2.2, and their results are given in Table 4. Additionally, in Table 4, the mean experimental capacity of each configuration, $F_{f,mean}$, and the relative difference with the numerical results are given, showing that the model is in good agreement with the test results and can evaluate the failure load with good accuracy.

Furthermore, the results of the simulations for the M170 and V170 configurations are given in Figures 7 and 8, respectively, in terms of force vs. displacement curves and compared with the experimental results. The force is the load applied in the model, and the deflection is the displacement measured at mid-span. In Figures 7 and 8, the dash-dotted lines represent the experimental results while the continuous lines represent the results obtained from the simulations. Additionally, in the plots the mean failure load obtained from the experiments is depicted with a horizontal dash-dotted line.
The curves in Figures 7 and 8 show good agreement between the experimental and the numerical results. Nevertheless, the stiffness of the simulated beams is slightly higher than in the experiments. The deflection in the experimental investigation is the measured movement of the loading actuator. Thus, the deflection is affected from the flexibility of the test rig, leading to a measured value slightly larger than in the idealized numerical model.

Table 4: *Comparison between numerical and experimental results*

Series	$F_{f,num}$ [kN]	$F_{f,mean}$ [kN]	Relative difference
M170	14.08	13.33	5.6%
V170	15.53	15.33	1.3%
M160	14.81	15.69	5.6%
V160	16.63	17.70	6.0%
M150	15.59	16.52	5.6%
V150	17.69	17.68	0.1%

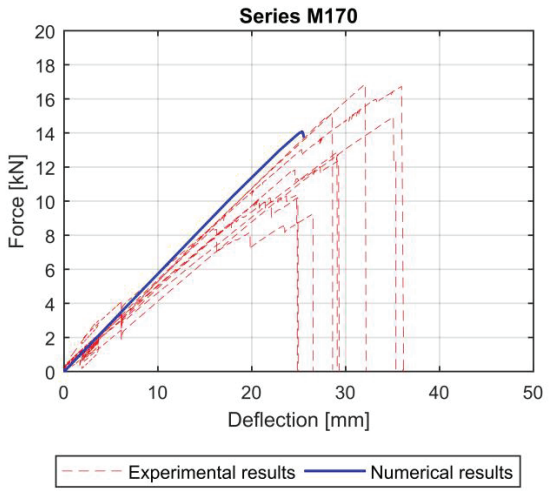

Figure 7: *Comparison between experimental results and numerical simulations: series M170.*

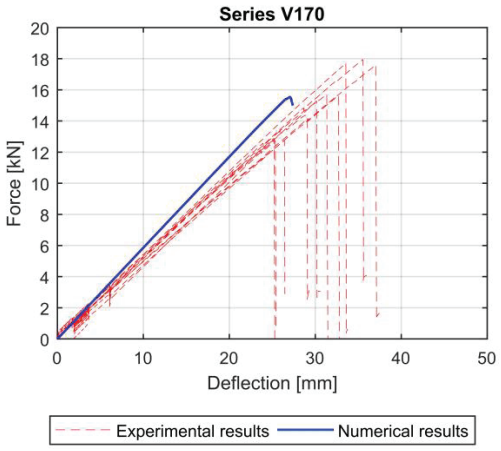

Figure 8: *Comparison between experimental results and numerical simulations: series V170.*

3.3 COMPARISON WITH REGULATIONS

The new generation of Eurocode 5 [9] includes normative regulations for the evaluation of timber member with holes. However, the diameter of the hole is limited to 30% of the beam height in case of unreinforced holes [9]. Herein, the Eurocode equations are however applied for holes with diameter larger than the limit. According to the new draft of Eurocode 5, the characteristic capacity F_k of a timber beam resembling load conditions and geometry of the tested beams is evaluated by taking into account the three conditions expressed in Equations (3), (4) and (5).

https://doi.org/10.52202/069179-0307

$$F_k = \frac{b \cdot \left(\frac{4 \cdot V_{\text{ref}}}{b \cdot d^2}\right)^{0.2}}{\frac{7}{52 \cdot h} \cdot \left[3 - \left(0.7 \cdot \frac{d}{h}\right)^2\right] \cdot \left[1.1 + 1.3 \cdot \frac{d}{h} - 1.3 \cdot \left(\frac{d}{h}\right)^2\right] + \frac{0.9 \cdot (l_A + d)}{8 \cdot d \cdot h} \cdot \left(\frac{d}{h}\right)^2} \cdot f_{\text{t,90,k}} \; ; \; V_{\text{ref}} = 0.01 \text{ m}^3 \quad (3)$$

$$F_k = \frac{2 \cdot b \cdot (h^3 - d^3)}{6 \cdot (l_A + d) \cdot h} \cdot f_{\text{m,k}} \quad (4)$$

$$F_k = \frac{2 \cdot b \cdot (h - 0.7 \cdot d)}{1.5 \cdot 1.8 \cdot \left(1 + 0.7 \cdot \frac{d}{h}\right) \cdot \left(\frac{0.7 \cdot d}{h}\right)^{0.2}} \cdot f_{\text{v,k}} \quad (5)$$

Equation (3) limits the capacity due to the tensile stresses perpendicular to grain generated by the transfer of bending and shear stresses around the hole, while Equations (4) and (5) limit the capacity because of the bending stresses and shear stresses generated in the residual cross-section, respectively.

The characteristic values of the strength are chosen according to the Technical Approval for K-beams [21], i.e. the tensile strength perpendicular to grain $f_{\text{t,90,k}}$ is chosen as 0.4 MPa, the bending strength $f_{\text{m,k}}$ as 24 MPa and the shear strength $f_{\text{v,k}}$ as 3.5 MPa. By inserting these strength values and the geometric parameters given in Table 1 into Equations (3), (4) and (5), the characteristic capacity F_k is obtained for all tested configurations.

The results are summarized in Table 5, together with a comparison with the experimental results. Furthermore, it is given the relative difference δ between the experimental results and Eq. (3).

Table 5: *Comparison experimental results vs regulations*

Series	F_k [kN] Eq. (3)	F_k [kN] Eq. (4)	F_k [kN] Eq. (5)	$F_{f,k}$ [kN] (exp.)	δ [%]
M170	9.9	12.5	14.6	8.2	+17.3
V170	12.7	27.5	14.6	11.5	+9.3
M160	10.4	13.0	15.6	11.1	-6.8
V160	13.1	28.9	15.6	11.3	+13.6
M150	10.9	13.5	16.6	11.9	-8.2
V150	13.6	30.2	16.6	14.5	-5.8

It can be noted that also for the Eurocode regulations the critical failure mechanism in the beams is splitting perpendicular to grain starting from the edge of the holes, in accordance with the experiments.

The perpendicular to grain splitting failure mechanism, represented by Equation (3), gives a safe estimation for holes of 150 mm, i.e. $d/h = 0.5$. However, for larger holes, it overestimates the characteristic capacity of the beams up to 17%. Indeed, Equation (3) is only valid up to $d/h = 0.3$ for unreinforced holes, and it may need adjusting in order to consider round holes with large diameters.

4 CONCLUSIONS

The objectives of this study were to experimentally evaluate the capacity of glued-laminated timber beams with large round holes and to validate a numerical model for the description of such beams.

Six series of experiments were performed on glued-laminated beams having a hole of diameter varying between 50% and 56.7% of the beam height, for a total of sixty tests. The series differed in the location of the hole: the M-series exhibited a hole in a moment-dominated cross-section, while the V-series presented it in a shear-dominated cross-section. The experiments showcased that the beams have a mean capacity ranging between 13.3 and 16.5 kN for the M-series, and between 15.3 and 17.7 kN for the V-series, respectively. This resulted in a decrease of the capacity of the beam, with respect to a beam without holes, up to 43% when the hole is positioned in a moment-dominated area. On the other hand, the presence of holes in a shear-dominated area has a lower influence, with a drop of the capacity up to 33%.

A numerical model, which resembled the beams geometry, was utilized to study their capacity and fracture process. The model presents horizontal cohesive layers in the location of the predicted fracture planes. An additional vertical cohesive layer was introduced underneath the hole in order to take into account the possibility of longitudinal tensile failure of the beams. The mechanical parameters of the cohesive layers were either chosen according to experimental investigations performed on the beams (Technical Approval) or relevant literature. The model exhibited an overall good agreement. Indeed, the relative difference of the numerical model does not exceed 6%, thus allowing for a proper evaluation of the failure load. Therefore, the numerical model may be used for further studies on the topic of large round holes in timber joists.

Finally, an analytical evaluation of the characteristic capacity of the beams according to the future European regulations was provided. As expected, the splitting verification was the most restrictive and it provided a fair evaluation of the failure load, especially for 150 mm hole diameter. However, the limitations on the size of holes in beams in joisted floors appear to be restrictive, as the beams having circular holes of about 57% of the height

show a residual strength exceeding 57% relative to a beam without any hole.
Furthermore, for a joisted floor having beams with large hole in an area, the spacing between the beams can be halved and the strength of that area becomes unaltered. However, some precautions should be made to avoid drying cracks starting at the hole. Possible actions are painting the hole surface and screw reinforcement.

ACKNOWLEDGMENTS

The authors would also like to acknowledge Atis Degro, Pål Østen Solberg and Noh Weldeab, for their contribution in performing experimental tests and numerical simulations. Furthermore, the supply of the test beams from Inntre Kjeldstad AS is gratefully acknowledged.

REFERENCES

[1] Abrahamsen, R. and Malo, K.A., *Structural design and assembly of "treet" - A 14-storey timber residential building in Norway*, in *WCTE 2014 - World Conference on Timber Engineering*. 2014: Quebec City, Canada.

[2] Abrahamsen, R., *Mjøstårnet - 18 storey timber building completed*, in *24. Internationales Holzbau-Forum IHF*. 2018: Garmisch-Partenkirchen, Germany.

[3] Aicher, S. and Höfflin, L., *Runde Durchbrüche in Biegeträgern aus Brettschichtholz - Teil 1: Berechnung.* Bautechnik, 2001. 78(10): p. 706-715.

[4] CEN, *Eurocode 5: Design of timber structures – Part 1-1: General rules and rules for buildings*, in *EN 1995-1-1:2004*. 2004, Comité Européen de Normalisation

[5] DIN, *Nationaler Anhang - National festgelegte Parameter - Eurocode 5: Bemessung und Konstruktion von Holzbauten - Teil 1-1: Allgemeines - Allgemeine Regeln und Regeln für den Hochbau*, in *DIN EN 1995-1-1:2004/NA:2013*. 2013, Deutsche Institut für Normung e.V.

[6] SINTEF, *Trebjelkelag. Dimensjonering og utførelse.* 2011.

[7] Tapia, C. and Aicher, S., *Evaluation of design concepts for holes in glulam beams - comparison with test results.* Otto-Graf-Journal, 2019. 18: p. 329-344.

[8] Danzer, M., Dietsch, P., and Winter, S., *Round holes in glulam beams arranged eccentrically or in groups*, in *INTER International Network on Timber Engineering Research - Meeting 50*. 2017: Kyoto, Japan.

[9] CEN, *Eurocode 5: Design of timber structures – Part 1-1: General rules and rules for buildings*, in *prEN 1995-1-1:20XX*. 2021, Comité Européen de Normalisation

[10] Johannesson, B., *Design problems for glulam beams with holes: stresses and stress concentrations, fracture criteria, design considerations*, in *Department of Structural Engineering, Division of Steel and Timber Structures*. 1983, Chalmers University of Technology: Göteborg.

[11] Höfflin, L., *Runde Durchbrüche in Brettschichtholzträger – Experimentelle und theoretische Untersuchungen*, in *MPA Otto-Graf-Institute*. 2005, University of Stuttgart: Stuttgart.

[12] Aicher, S. and Höfflin, L., *Tragfähigkeit und Bemessung von Brettschichtholzträgern mit runden Durchbrüchen – Sicherheitsrelevante Modifikationen der Bemessungsverfahren nach Eurocode 5 und DIN 1052.*, in *MPA Otto-Graf-Institute*. 2006, University of Stuttgart: Stuttgart.

[13] Danzer, M., Dietsch, P., and Winter, S., *Reinforcement of round holes in glulam beams arranged eccentrically or in groups*, in *WCTE 2016 - World Conference on Timber Engineering*. 2016: Wien, Austria.

[14] Aicher, S., Schmidt, J., and Brunold, S., *Design of timber beams with holes by means of fracture mechanics*, in *CIB-W18/28*. 1995: Copenhagen, Denmark.

[15] Aicher, S. and Höfflin, L., *Fracture behavior and design of glulam beams with round holes*, in *WCTE 2008 - 10th World Conference on Timber Engineering*. 2008: Miyazaki, Japan. p. 132-140.

[16] Danielsson, H. and Gustafsson, P.J., *A probabilistic fracture mechanics method and strength analysis of glulam beams with holes.* European Journal of Wood and Wood Products, 2011. 69(3): p. 407-419.

[17] Schmidt, J. and Kaliske, M., *Models for numerical failure analysis of wooden structures.* Engineering Structures, 2009. 31(2): p. 571-579.

[18] Ardalany, M., Fragiacomo, M., and Moss, P., *Modeling of Laminated Veneer Lumber Beams with Holes Using Cohesive Elements.* Journal of Structural Engineering, 2016. 142(1): p. 04015102.

[19] Danielsson, H. and Gustafsson, P.J., *Fracture analysis of glued laminated timber beams with a hole using a 3D cohesive zone model.* Engineering Fracture Mechanics, 2014. 124-125: p. 182-195.

[20] CEN, *Timber structures - Glued laminated timber and glued solid timber*, in *EN 14080:2013*. 2013, Comité Européen de Normalisation

[21] SINTEF, *Teknisk Godkjenning K-bjelken*. 2014, SINTEF Byggforsk: Oslo.

[22] INSTA, *Nordic visual strength grading rules for timber*, in *INSTA 142:2009*. 2009, Internordic Standardization.

[23] CEN, *Structural timber - Strength classes*, in *EN 338:2016*. 2016, Comité Européen de Normalisation

[24] CEN, *Timber structures - Test methods - General principles for static load testing*, in *EN 380:1993*. 1993, Comité Européen de Normalisation

[25] Dassault Systemes, *Abaqus/CAE*, in *Abaqus*. 2014.

[26] Dahl, K.B., *Mechanical properties of clear wood from Norway spruce*, in *Faculty of Engineering Science and Technology, Department of Structural*

https://doi.org/10.52202/069179-0307

Engineering. 2009, Norwegian University of Science and Technology: Trondheim.
[27] Massaro, F.M., Stamatopoulos, H., Andersen, J., and Brekke-Rasmussen, E., *Finite element modelling and experimental verification of timber halved and tabled scarf joints.* International Wood Products Journal, 2022: p. 1-10.
[28] Norsk Treteknisk Institutt, *Skjærtest av K-bjelken*. 2003, Norsk Treteknisk Institutt: Oslo.
[29] Norsk Treteknisk Institutt, *Bøyetest av K-bjelken*. 2003, Norsk Treteknisk Institutt: Oslo.
[30] Norsk Treteknisk Institutt, *Test av K-bjelken*. 2009, Norsk Treteknisk Institutt: Oslo.
[31] JCSS, *Jcss Probabilistic Model Code*, in *Part 3: Resistance Models*. 2006, Joint Committee on Structural Safety. p. 16.
[32] Schoenmakers, J.C.M., *Fracture and failure mechanisms in timber loaded perpendicular to the grain by mechanical connections*. 2010, Eindhoven University of Technology: Eindhoven.
[33] Ostapska, K., *Fracture in wood of Norway spruce*, in *Faculty of Engineering Science and Technology, Department of Structural Engineering*. 2020, Norwegian University of Science and Technology: Trondheim.
[34] Ostapska, K. and Malo, K.A., *Wedge splitting test of wood for fracture parameters estimation of Norway Spruce.* Engineering Fracture Mechanics, 2020. 232: p. 107024.
[35] Wu, E.M., *Application of Fracture Mechanics to Anisotropic Plates.* Journal of Applied Mechanics, 1967. 34(4): p. 967-974.
[36] Jernkvist, L.O., *Fracture of wood under mixed mode loading: I. Derivation of fracture criteria.* Engineering Fracture Mechanics, 2001. 68(5): p. 549-563.
[37] CEN, *Timber structures - Calculation and verification of characteristic values*, in *EN 14358:2016*. 2016, Comité Européen de Normalisation